Supporting Information

Bifunctional Nickel Ferrite Decorated Carbon Nanotubes Arrays as the Free-standing Air Electrode for Rechargeable Zn-air Batteries

*Ya Yan [a, §], Yangyang Xu [b, §], Bin Zhao [a, §], Yong Xu [a], Yan Gao [a], Guangda Chen [b], Weibo Wang [a], Bao Yu Xia [b, *]*

[a] School of Materials Science & Engineering, University of Shanghai for Science and Technology, 516 Jungong Road, Shanghai 200093, PR China

[b] Key Laboratory of Material Chemistry for Energy Conversion and Storage (Ministry of Education), Hubei Key Laboratory of Material Chemistry and Service Failure, School of Chemistry and Chemical Engineering, Wuhan National Laboratory for Optoelectronics, Huazhong University of Science and Technology (HUST), 1037 Luoyu Road, Wuhan 430074, PR China.

[§] These authors contributed equally.

*Corresponding author. E-mail: byxia@hust.edu.cn (B. Y. Xia)

Experimental Section

Synthesis of Vertically Aligned Carbon Nanotubes: In brief, the VACNTs array was grown in a tube furnace by water-assisted CVD at 820 °C. In this process, high-purity ethylene (99.99%, Shanghai Lingyi gas) was used as the carbon source and Ar (99.999%, Shanghai Lingyi gas) and H_2 (99.999%, Shanghai Lingyi gas) was worked as the carrier gases at 1 atm, and the total flow rate was controlled at 300 sccm. Fe film (1.5 nm)/Al_2O_3 film (30 nm) were consecutively deposited on Si substrate by Magnetron sputtering method, and they worked as catalysts to grow carbon nanotubes. In order to improve the lifetime of catalysts, a portion of Ar gas was passed through a water bubbler to bring out a little bit of water vapor. Typical CVD growth was conducted with 300 sccm (abbreviation of the standard cubic centimeter per minute) ethylene and a water

concentration of 100-200 ppm for 10 minutes at ambient pressure. Millimeter-long VACNT arrays consisting of nanotubes with average diameters of 10-15 nm was grown, and it is the raw material for the next synthesized steps.

***Fabrication of $NiFeO_x$@VACNTs*:** Typically, VACNTs was placed in a high-pressure reaction vessel of 50 mL first, the precursor Iron (III) acetylacetonate [$Fe(acac)_3$] purchased from Aldrich Chemical and nickelocene obtained from Alfa Aesar are both employed as received, and they were used as precursors to synthesize $NiFe_2O_4$. First step, 36 mg $Fe(acac)_3$ and 10 mg nickelocene (Ni/Fe molar ratio of 1:2) were added to the container in the vessel, then, 0.5 mL benzene solution (worked as solvent) was also added to this container dropwise. The above two procedures were achieved in a glove box filled with N_2, preventing precursor from being contaminated by air. Then, the vessel is sealed tightly and then connected to the gas pipeline. After the reactor was preheated to 50 °C, CO_2 was slowly introduced by a syringe pump to reach the targeted pressure. After that, the vessel was heated and kept at 100 °C for 6 hours to create a closed space with high temperature and pressure, where the precursor was completely dissolved into the $SCCO_2$ fluids and then adsorbed into the dense VACNTs. Then the $SCCO_2$ was released from the reactor over a period of approximately 2 h, the reaction system cooled and depressurized to room temperature slowly. After this treatment, precursor was dissolved into the $SCCO_2$ fluids and adsorbed into the VACNTs array completely. The amount of adsorbed precursor was determined by weighing the VACNT before and after $SCCO_2$ treatment. The precursor impregnated VACNTs were subsequently transferred to the oven of rapid thermal annealing (RTP) furnace and annealed at 550°C, 600 °C and 650 °C in vacuum environment, respectively, after that the precursor absorbed in VACNTs was converted to oxygen vacancy-rich $NiFeO_x$ nanoparticles. Note that the weight percentages of $NiFeO_x$ in the composite was confirm to be 20wt% by the TGA curves.

Characterizations: Crystal structures of the composite was analyzed by X-ray diffraction (XRD, Advance D8). Raman spectra was taken on a Raman Station 400F with an excitation length of 532 nm. Morphologies of the samples were observed with field-emission scanning electron microscopy (FE-SEM, Quanta FEG450)

and transmission electron microscopy (TEM, JEM-2010F, Germany). Pore structure of the $NiFe_2O_4$/VACNT samples were measured by nitrogen adsorption-desorption isotherms performed at 77 K on a Micrometritics ASAP-2020 volumetric adsorption system, the specific surface area was calculated by Brunauer-Emmett-Teller (BET) method. To determine exact loading amounts of $NiFe_2O_4$ on carbon nanotubes, thermogravimetric analysis (TGA, Pyris 1 TGA, Perkin-Elmer) was carried out in air. EDS (JEOL-2010) and XPS (PHI 5000C ESCA System) measurements were conducted to investigate compositions of the samples.

Preparation of working electrode: The $NiFeO_x$@VACNTs hybrids were detached from the original Si substrate by cutting, then it was transferred to nickel foam (Latech) and directly pressed on nickel mesh with a pressure of 4 MPa. Therefore, the working electrode was constructed without using any binders. The loading amount of $NiFeO_x$@VACNTs composite was measured to be 3.5 mg cm^{-2}. For meaningful comparisons, we prepared 20% Pt/C (Alfa Aesar) and IrO_2 (Alfa Aesar) on the nickel mesh (denoted as Pt/C and IrO_2) with the same mass loading. In brief, 3.5 mg 20% Pt/C or IrO_2 were dispersed in a 2 mL mixture solution containing 800 μL water, 120 μL 5% Nafion solution, and 1.08 mL ethanol, followed by sonication for 20 minutes to obtain a homogeneous catalyst ink. Then the catalyst ink was loaded on the Ni Foam (NF) (1 cm x 1 cm) for many times. Consequently, the overall loading amount is about 3.5 mg cm^{-2}.

Electrochemical measurement: The electrochemical measurements were carried out in a conventional three-electrode on an electrochemical workstation (Autolab 302N) with the Ni foam loaded electrocatalysts as working electrodes, a graphite rod as the counter electrode and Ag/AgCl as the reference electrode. All the electrochemical tests were conducted in 0.1 M KOH solution and all potentials reported in this paper were calibrated with respect to the reversible hydrogen electrode (RHE) according to the Nernst equation ($E_{RHE} = E_{Ag/Ag/Cl} + 0.059 \times pH + 0.20$). For the oxygen evolution reaction, the linear sweep voltammetry curves were recorded in a potential range of 1.1 V to 1.7 V at a rate of 5 mV s^{-1} at static condition. For the oxygen reduction reaction, the cycle voltammetry and linear sweep voltammetry test were carried out in O_2-saturated 0.1 M KOH solution and were scanned cathodically from 1.1 to 0.4 V at a rate of 5 mV s^{-1}. In the Tafel plots of E

vs. Log (J_k), the kinetic current density was calculated from the mass-transport correction of the working electrode: $J_k = J*J_L/(J_L-J)$, where J is the measured current density (mA cm^{-2}), J_L is the diffusion-limiting current densities (mA cm^{-2}).

***Zn-air batteries assembly and test*:** The prepared air electrode and a polished Zn foil (3 mm) were assembled in 6.0 M KOH and 0.2 M zinc acetate electrolyte. For the liquid Zinc-air batteries test, galvanostatic discharge-charge curves were recorded using a LAND testing station at a current density of 5 mA cm^{-2} with 20 min per cycle (charge 10 min and discharge 10 min). For solid-state Zinc-air batteries, the free-standing catalysts (3.5 mg cm^{-2}) were directly used as air electrode, a gel polymer electrolyte was prepared by mixing 5 ml of 11.25 M KOH and 0.25 M ZnO with 0.5 g acrylic acid and 0.075g N, N'-methylene-bisacrylamide (MBA) having 75 µL saturated $K_2S_2O_4$ as the initiator. In brief, 5 mL of 11.25 M KOH and 0.25 M ZnO was mixed with 0.5 g of acrylic acid and 0.075g N, N'-methylene-bisacrylamide (MBA). The white precipitate was filtered out after 20 min of stirring. Then, 75 µL saturated $K_2S_2O_4$ as the initiator was added into the solution and a small portion of the solution was poured into the void of acrylic tape once the solution started to polymerize. All the measurements were performed at a current density of 1 mA cm^{-2} with 20 min per cycle on a LAND battery testing system.

Figures and captions

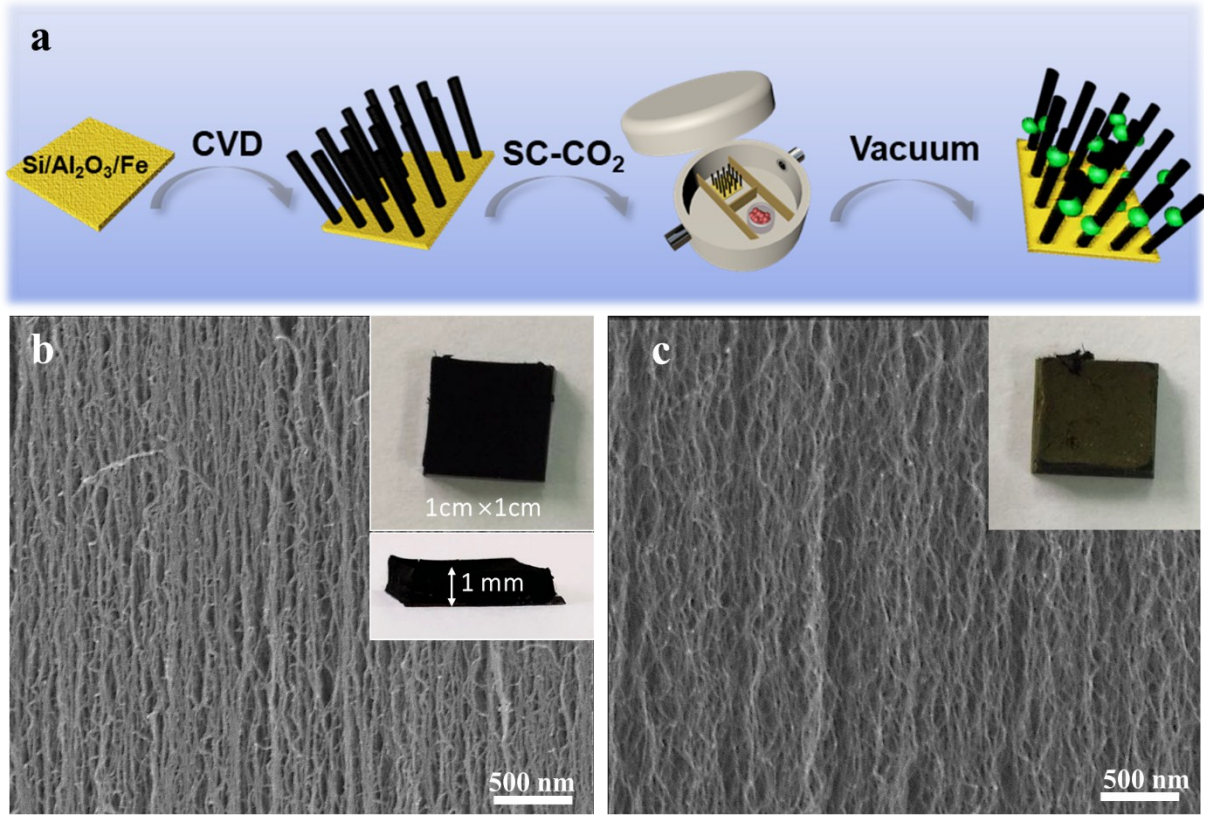

Figure S1. (a) Synthesis procedure for the $NiFeO_x$@VACNTs. SEM images of as-synthesized VACNTs (b) and the nickelocene/$Fe(acac)_3$/VACNTs precursors after $SCCO_2$ treatment (c).

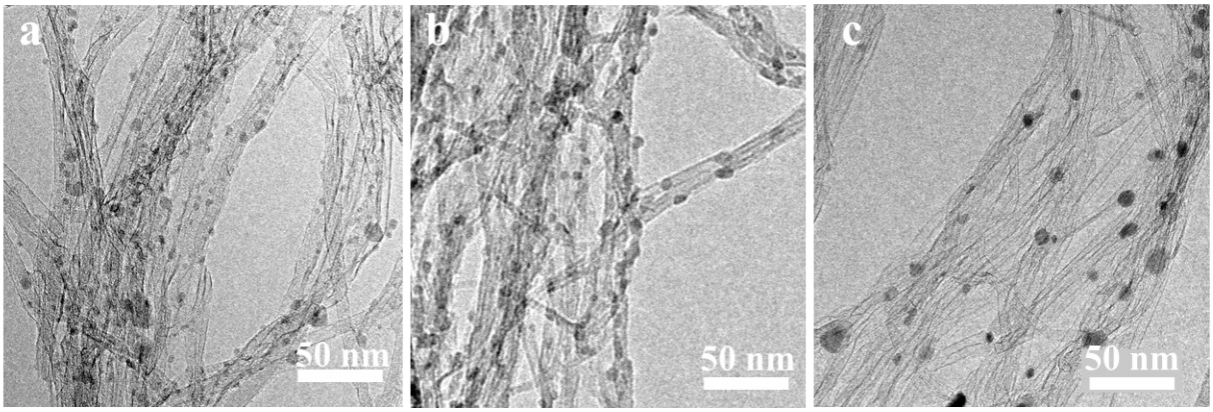

Figure S2. TEM images of NiFeOx@VACNTs onatined at 550 °C, 600°C, 650°C.

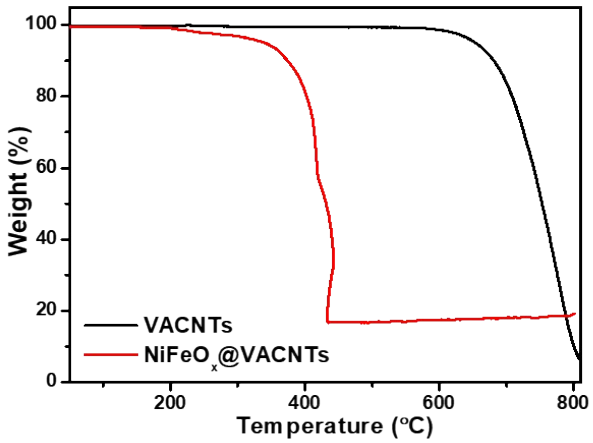

Figure S3. Thermogravity curves of NiFeOx/VACNTs composites and pure VACNTs.

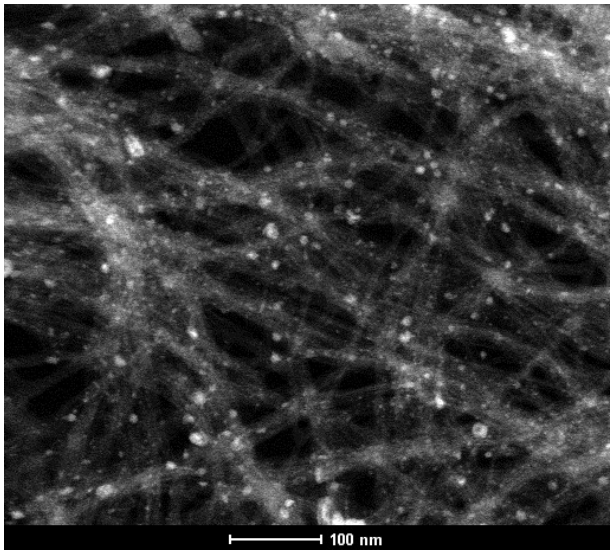

Figure S4. Dark-field high-resolution TEM image showing highly dispersed NiFeOx nanoparticles in

VACNTs.

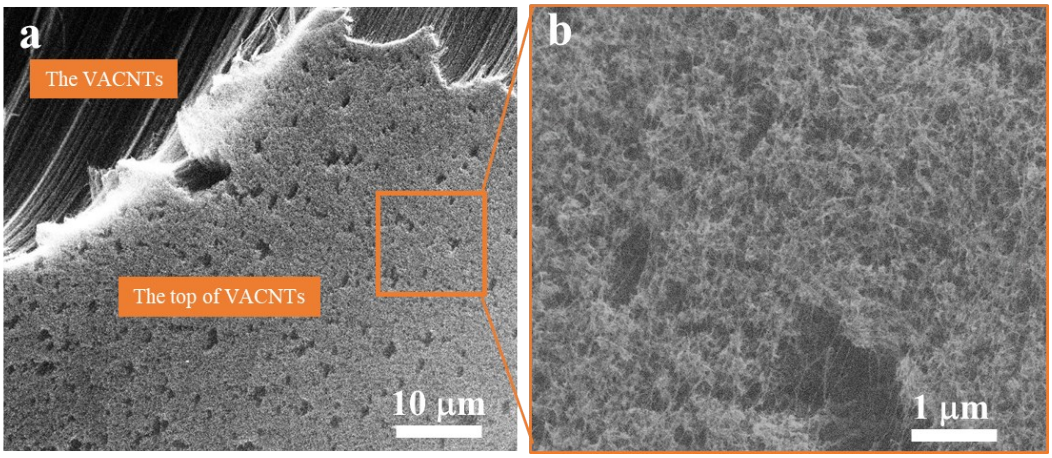

Figure S5. SEM images for NiFeOx/VACNTs mixture.

NiFeOx/VACNTs mixture was synthesized by adding $NH_3 \cdot H_2O$ (6mL, 30%) dropwise to the aqueous solution (34 mL) containing $FeSO_4 \cdot 7H_2O$ and $NiSO_4 \cdot 6H_2O$ (Ni/Fe molar ratio of 1:2) and then the as-obtained solution was transferred into a stainless-steel vessel with a piece of $SCCO_2$ treated VACNTs, which was subjected to the hydrothermal reduction at 180 °C for 12 h. Finally, the NiFeOx/VACNTs was obtained by annealing the precursor at 600 °C in vacuum environment.

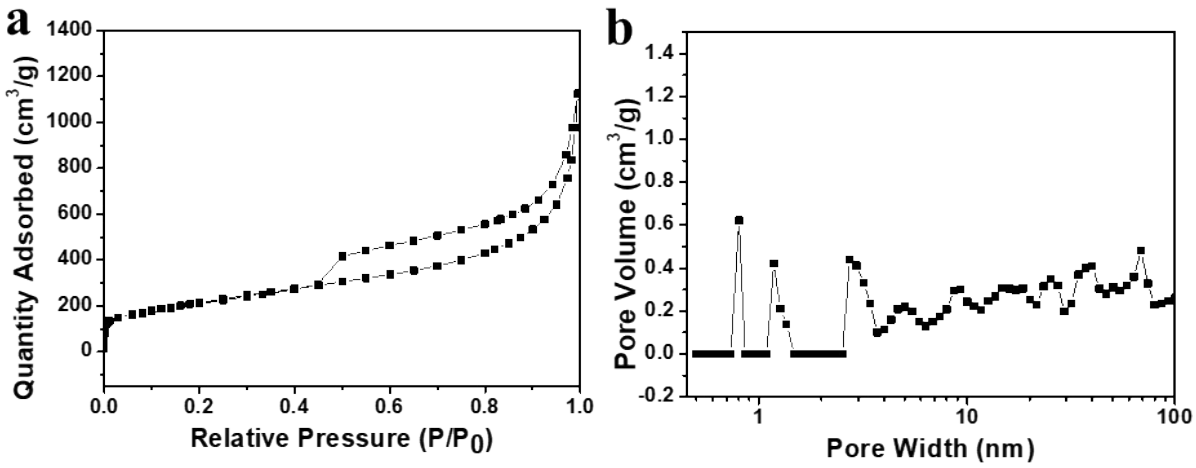

Figure S6. (a) N_2 adsorption-desorption isotherms (a) and the pore size distribution (b) of NiFeOx@VACNTs.

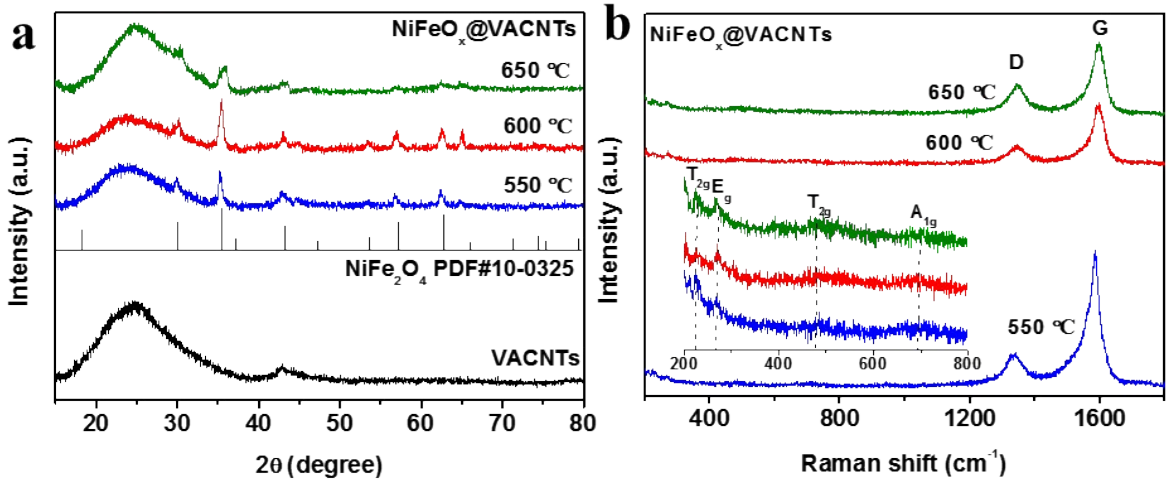

Figure S7. XRD patterns (a) and Raman spectra (b) of NiFeOx@VACNTs.

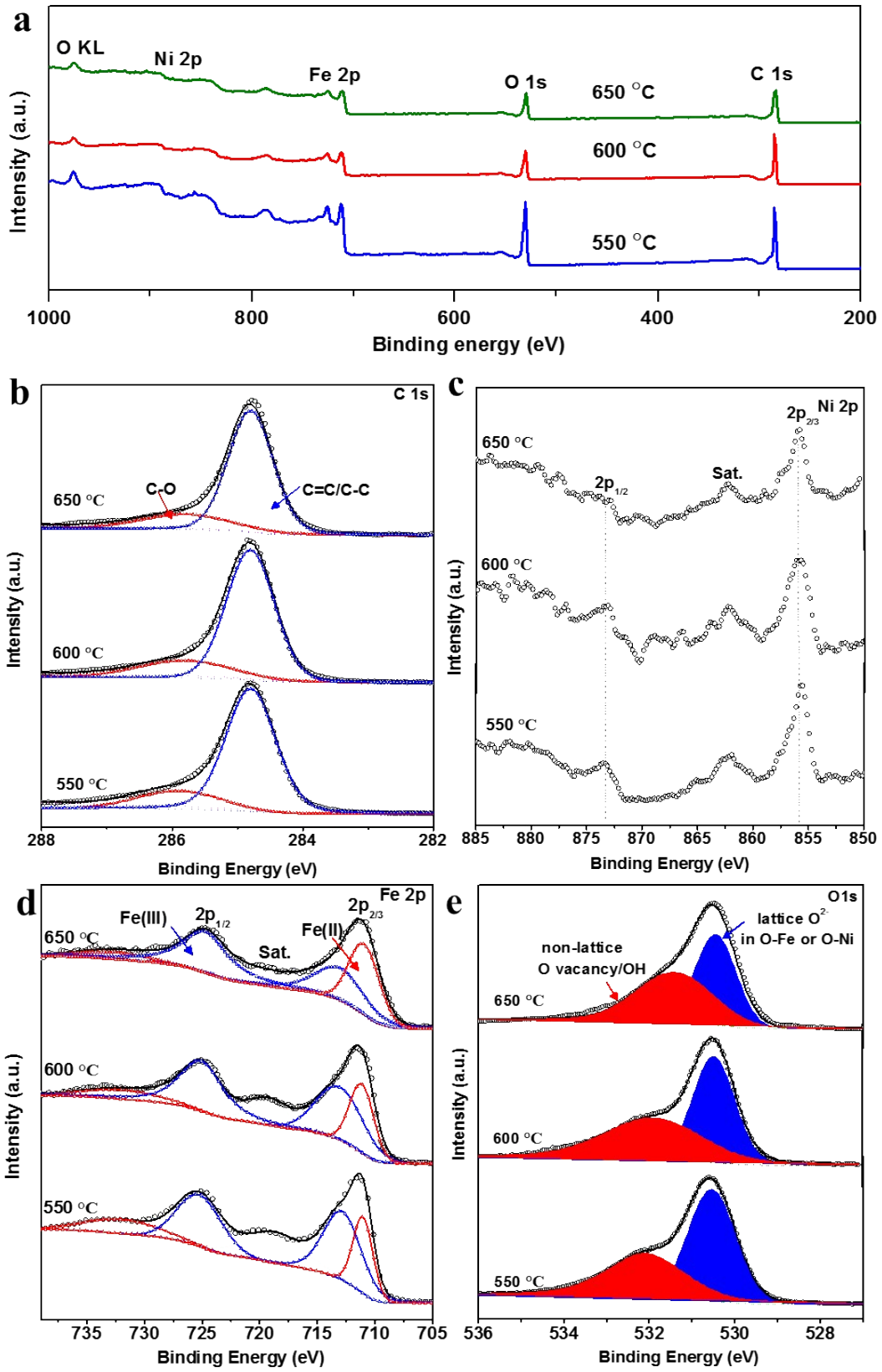

Figure S8. XPS full survey (a) and high-resolution XPS spectra of C 1s (b), Ni 2p (c), Fe 2p (d) and O 1s (e) for NiFeOx@VACNTs prepared at different temperature.

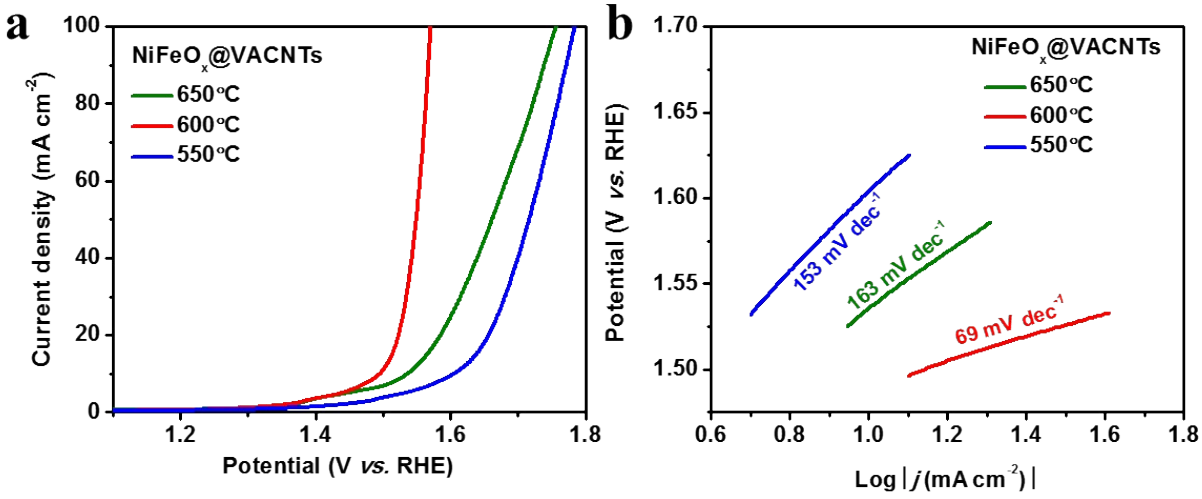

Figure S9. OER polarization curves (a) and the corresponding Tafel plots (b) of NiFeOx@VACNTs prepared at different temperature.

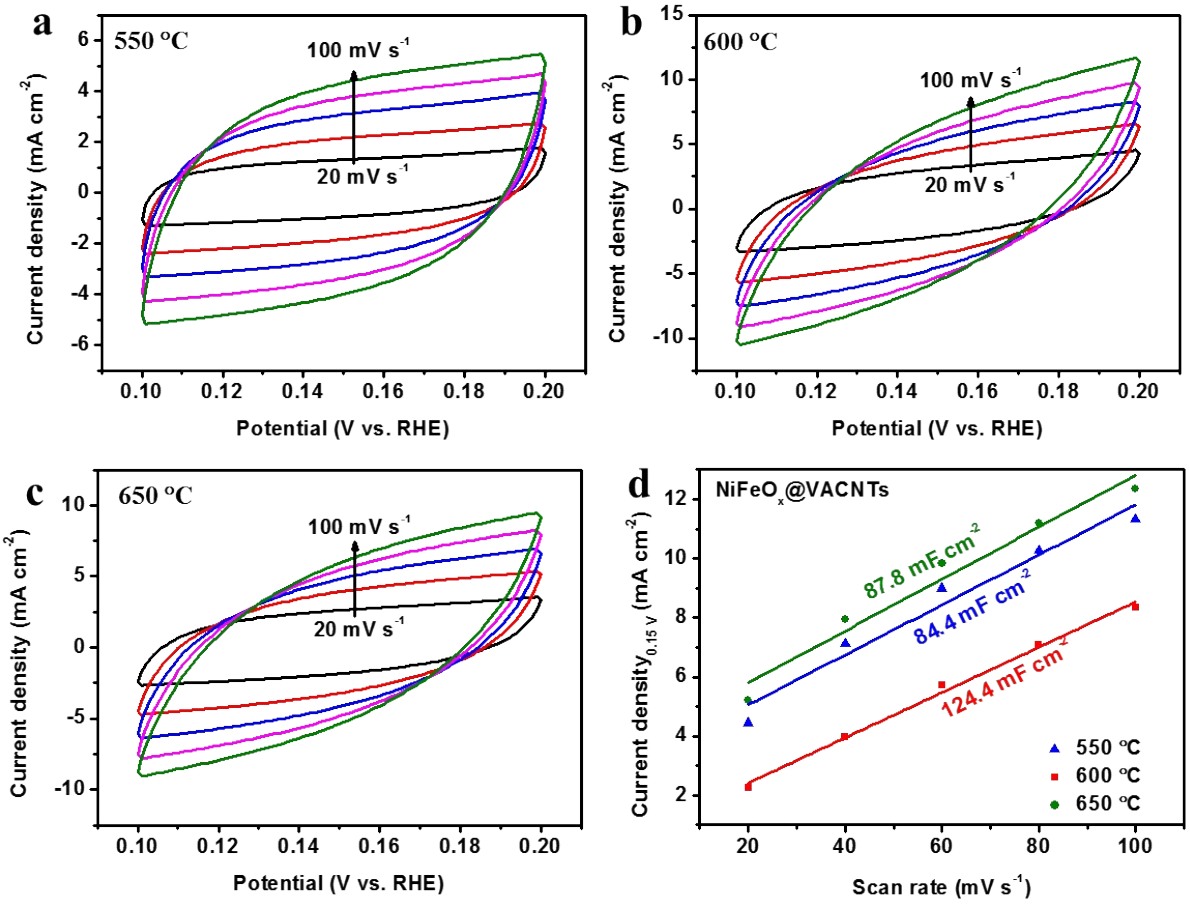

Figure S10. CV curves of NiFeOx@VACNTs obtained in a non-faradaic capacitance current range at different scan rates (a-c). The capacitive currents at 0.15 V (vs. RHE) as a function of scan rates**.**

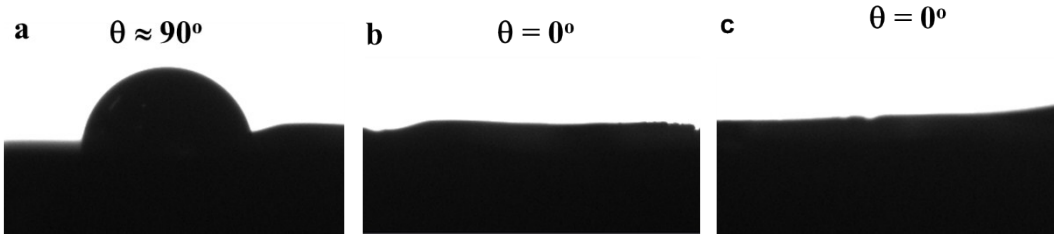

Figure S11. Contact angle measurement for (a) as-grown VACNTs, (b) $SCCO_2$ treated VACNTs and (c) $NiFeO_x$@VACNTs.

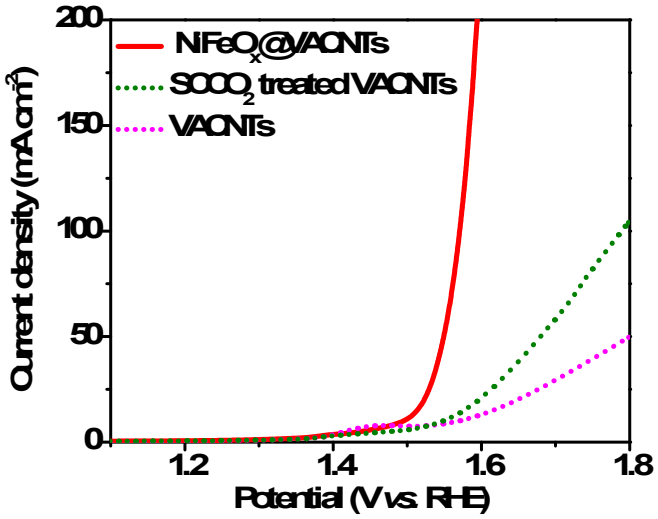

Figure S12. OER polarization curves of as-grown VACNTs, $SCCO_2$ treated VACNTs and $NiFeO_x$@VACNTs.

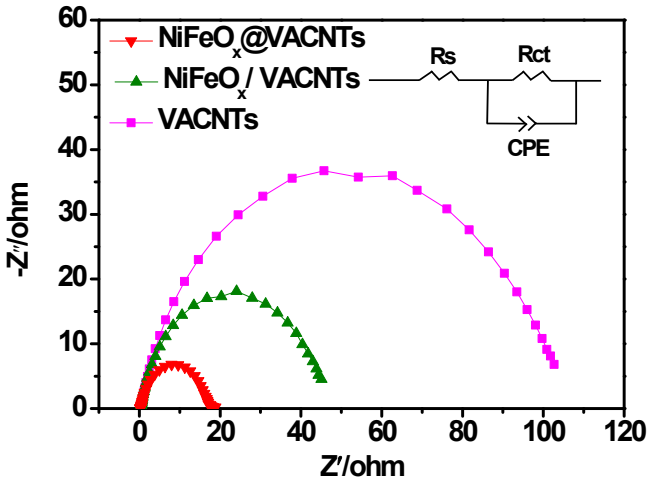

Figure S13. Nyquist plots of various catalysts with a fitted equivalent circuit (inset) at a potential of 1.55 vs. RHE.

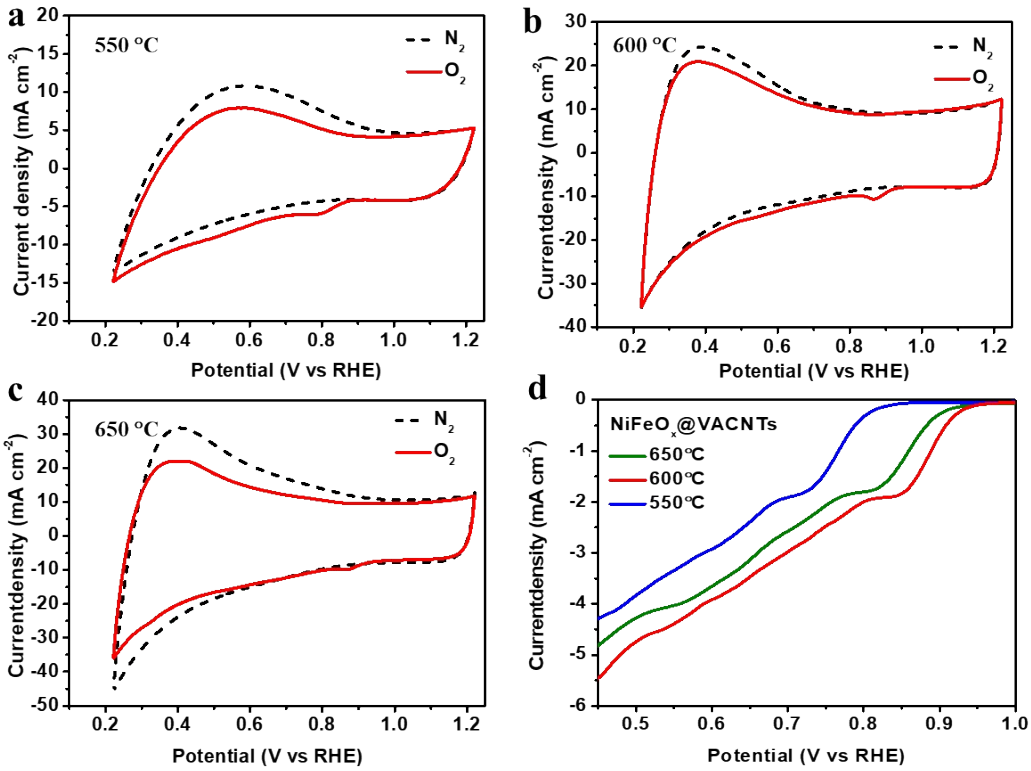

Figure S14. CV curves (a-c) and ORR polarization curves (d) of NiFeOx@VACNTs annealed at different temperature, which are recorded in N_2 (or O_2)-saturated 0.1 M KOH solution.

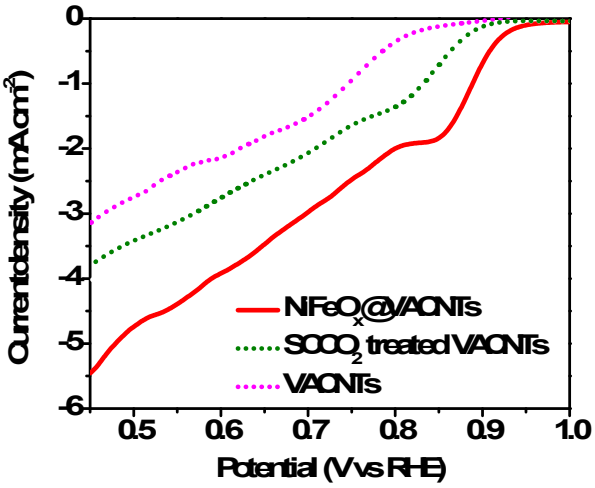

Figure S15. ORR polarization curves of $SCCO_2$ treated VACNTs in comparison to the as- prepared the VACNTs.

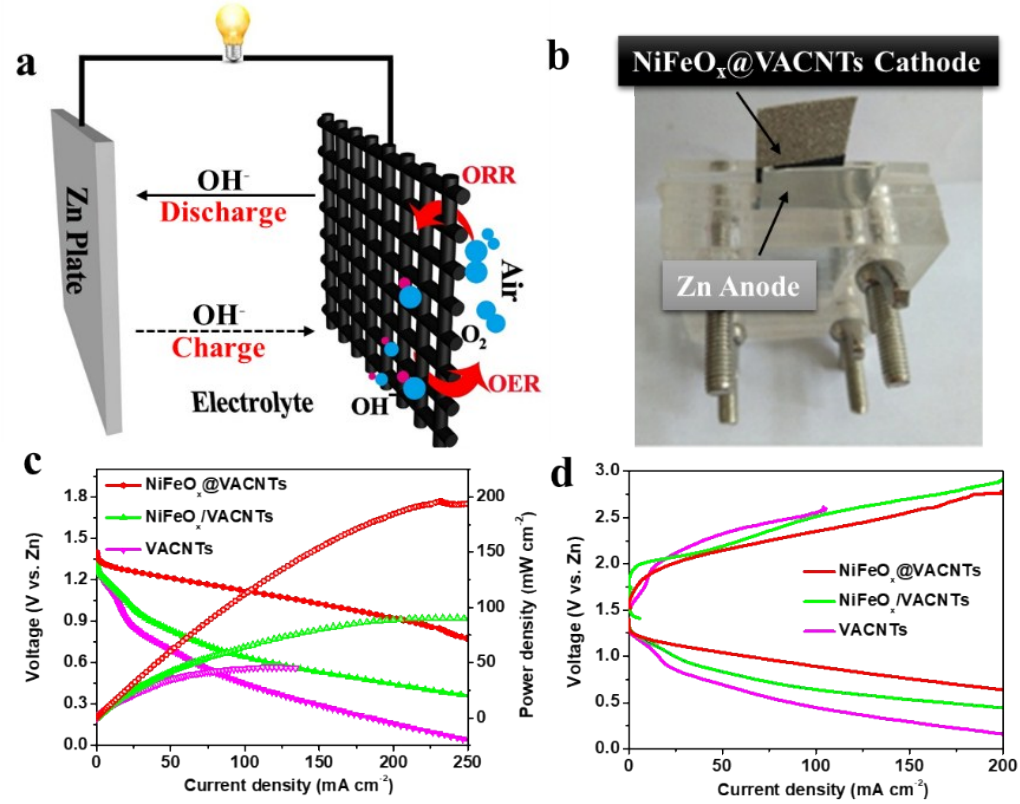

Figure S16. Scheme of the Zn-air battery (a). Photograph of a Zn-air battery assembled with the NiFeOx@VACNTs film electrode (b). Discharge polarization curves and the corresponding power density curves (c) and charge and discharge polarization curves (d) for Zn-air battery with different catalysts.

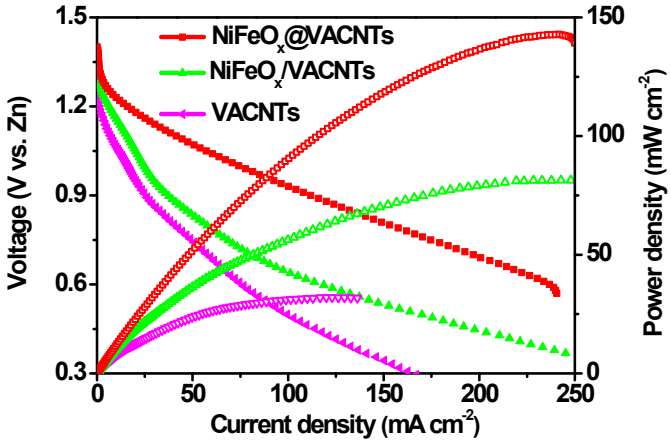

Figure S17. Discharge polarization curves and the corresponding power density curves for solid-state Zn-air battery with different catalysts.

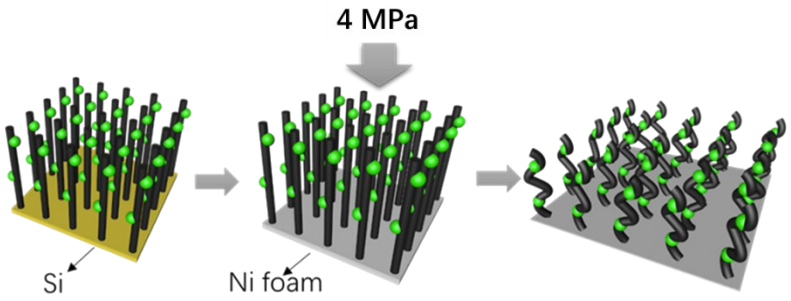

Figure S18. Preparation process of the NiFeOx@VACNTs electrode.

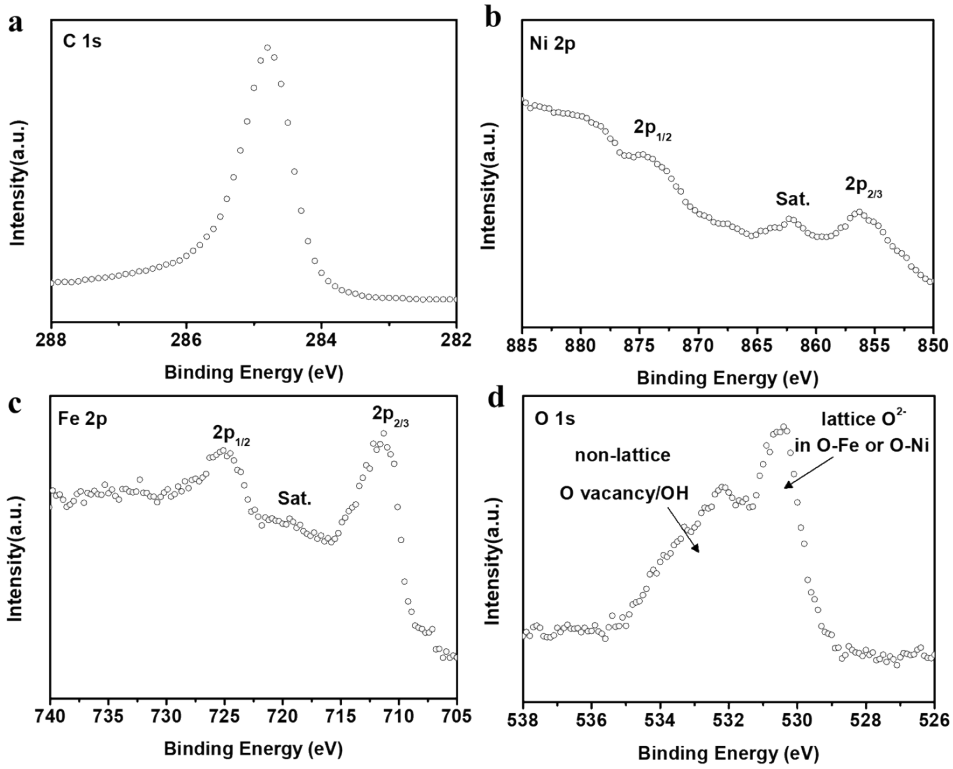

Figure S19. XPS of C 1s (a), Ni 2p (b), Fe 2p (c) and O 1s (d) for NiFeOx@VACNTs (600 ºC) after stability test for OER.

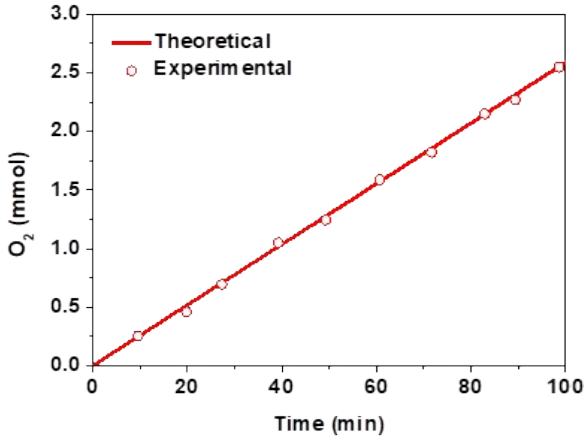

Figure S20. Faradic efficiency of the OER in 0.1 M KOH at η =340 mV.

Table S1. Summary of various bifunctional electrocatalysts for liquid Zn-air battery.

Catalyst	Discharge current density (mA cm^{-2}) at 1.0 V	Power density (mW cm^{-2})	Specific capacity (mAh g^{-1}) @J (mA cm^{-2})	Cycle Numbers @J (mA cm^{-2})	Cycle Time (h)	Reference
NiFeOx@ VACNTs	**161**	**194**	**-800@5**	**9000@5**	**1500**	**This work**
Pt/C+IrO_2	**78**	**105**	**-618@5**	**360@5**	**120**	**This work**
$NiCo_2S_4$@ g-C_3N_4-CNT	~80	142	486@10 493@20	330@10	110	*Adv. Mater.* **2019**, 1808281
Co_2FeO_4 /NCNTs	~45	91	605@50	600@50	100	*Angew. Chem. Int. Ed.* **2019**, 10.1002/ange.201907595
Ni-Fe-MoN NTs	~30	118	754@10	100@10	20	*Adv. Energy Mater.* **2018,** *8,* 1802327
CoNiFe-S MNs	~40	140		120@2	40	*Adv. Energy Mater.* **2018**, *8*, 1801839
$NiCo_2S_4$ /N-CNT	107	147	431@10	150@10	100	*Nano Energy*, **2017,** *31,*541-550
FeN_x/C-700-20	~18	36		504@5	84	*Adv. Energy Mater.* **2018**, *8*, 1800955
S-GNS /$NiCo_2S_4$	~90	216		150@10	100	*Adv. Funct. Mater.* **2018**, *28*, 1706675
FeP_x/Fe-N-C/NPC			739@20	168@20	33	*Adv. Energy Mater.* **2018**, 1803312
Meso/micro-FeCo-N_x-CN-30	~60	150		20@10	40	*Angew. Chem. Int. Ed.* **2018**, *57*, 1856
NCNT/CoO-NiO-NiCo	~42		597@7 545@20	96@20	16	*Angew. Chem. Int. Ed.* **2015**, *127*, 9790
$Fe_{0.5}Co_{0.5}O_x$/ NrGO	~50	86	756@10 709@25	60@10	120	*Adv. Mater.* **2017**, 1701410
CoFe /N-GCT	~160	203		1600@10	267	*Angew. Chem. Int. Ed.* **2018,** *130*, 16398
C@NCF -900	~110			200@50	33	*Adv. Mater.* **2018**, *30*, 1803372
DN-CP@G	~100	135	591@20	250@5	~	*Adv. Energy*

						Mater. **2018**, *8*, 1703539
$CoIn_2S_4$/S-rGO	~80	133	745@5	150@10	50	*Adv. Energy Mater.* **2018**, *8*, 1802263
$CuCo_2O_4$ /N-CNTs	~48	84	817@10	~@20	40	*Adv. Funct. Mater.* **2017**, *27*, 1701833
Cu_3P@NPPC-650	~70	111		222@5	37	*Adv. Mater.* **2017**, 1703711
N-GCNT /FeCo	~50	89	872@10	240@ 120	40	*Adv. Energy Mater.* **2017**, *7*, 1602420
CoNi/BCF	~80	155	711@10	90@10	30	*Applied Catalysis B: Environmental* **2019***,240,* 193-200
NPCS-900	~50	79	684@2	337@2	55	*Nano Energy* **2019,** *60***,**536-544
			625@20	245@20	40	
CoN_4/NG	~80	115	730@10	150@10	100	*Nano Energy* **2018,** *50***,**691-698
3D-CNTA	~110	157		240@10	40	*Nano Energy* **2017***,39* 626-638
NCNT /$Co_xMn_{1-x}O$	~15		581@7	~@7	12	*Nano Energy*, **2016,** *20,*315-325
CoP@ mNSP-C	~80	124		100@1	450	*Small,* **2017**, *13,* 1702068
				120@20	80	

Table S2. Summary of various bifunctional electrocatalysts for flexible solid-state Zn-air battery.

Air catalyst	Open-circuit potential	Discharge current density (mA cm^{-2}) at 1.0 V	Peak power density (mW cm^{-2})	Cycle Numbers @ J (mA cm^{-2})	Cycle Time (h)	Reference
NiFeOx@ VACNTs	**1.50**	**78**	**227**	**180@1**	**60**	**This work**
Pt/C+IrO_2	**1.40**	**53**	**88**	**36@1**	**12**	**This work**
$NiFe_2O_4$ /CNTs		~25	56	60@5	10	*Nano Energy* **2019,** *57,* 176-185
NiO/CoN PINWs	1.34			25@1	8	*ACS Nano,* **2017,** *11*, 2275-2283
1 nm-CoO_x	1.39	~55		60@6	10	*Adv. Mater.* **2019**, *31*, 1807468
ultrathin Co_3O_4/CC	1.33	~12		30@2	10	*Adv. Energy Mater.* **2017**, *7*, 1700779
NC-Co_3O_4 -90	1.44	~75	82	52@1	17	*Adv. Mater.* **2017**, 1704117
CC-AC	1.37	~28	52	50@1	17	*Adv. Energy Mater.* **2018**, 1802936
N-GCNT /FeCo-3	1.25	~48	98	36@1	12	*Adv. Energy Mater.* **2017**, *7*, 1602420
NGM-Co	1.44	~20	30			*Adv. Mater.* **2017**, *29*, 1703185
CMS/NCN F		~9		21@5	7	*Nanoscale*, **2017**, *9*, 15865–15872
Co/Co-N-C	1.41			60@2	10	*Adv. Mater.* **2019**, 1901666
$CuCo_2S_4$ NSs	1.20			63@1	21	*Nanoscale*, **2018,** *10*, 6581-6588